tvst

Retina

Identification of Novel Retinal Pericyte-Targeting rAAV Vectors Through Directed Evolution

Dwani D. Patel[1,2,*], Damien Marsic[3,4,*], Ramesh Periasamy[2], Sergei Zolotukhin[3], and Daniel M. Lipinski[1,2]

[1] Department of Cell Biology, Neurobiology and Anatomy, Medical College of Wisconsin, Milwaukee, WI, USA
[2] Department of Ophthalmology and Visual Science, Medical College of Wisconsin, Milwaukee, WI, USA
[3] Department of Pediatrics, University of Florida College of Medicine, Gainesville, FL, USA
[4] Porton Advanced Solutions, Suzhou, Jiangsu, China

Correspondence: Daniel M. Lipinski, Department of Cell Biology, Neurobiology and Anatomy, Medical College of Wisconsin, 8701 Watertown Plank Road, Milwaukee, WI 53226, USA.
e-mail: dlipinski@mcw.edu

Received: November 29, 2021
Accepted: July 21, 2022
Published: August 26, 2022

Keywords: AAV; gene transfer; retinal pericytes

Citation: Patel DD, Marsic D, Periasamy R, Zolotukhin S, Lipinski DM. Identification of novel retinal pericyte-targeting rAAV vectors through directed evolution. Transl Vis Sci Technol. 2022;11(8):28, https://doi.org/10.1167/tvst.11.8.28

Purpose: Retinal pericytes play a vital role in maintaining retinal homeostasis, and their dysfunction underlies pathogenesis in such vascular eye diseases as diabetic retinopathy and wet age-related macular degeneration. Consequently, retinal pericytes are attractive therapeutic targets for gene therapy, but effectively targeting pericytes with recombinant adeno-associated virus (rAAV) vectors remains a challenge.

Methods: We introduced genetic modifications into the surface-exposed variable regions of the rAAV2/2 capsid to generate a complex library ($>1 \times 10^7$) of capsid mutants that were then screened for preferential tropism toward retinal pericytes. Using the Tg(Cspg4-DsRed.T1)1Akik/J reporter mouse model, which has red fluorescent pericytes that can be isolated via flow cytometry in order to recover vector genomes, we performed three rounds of screening and identified seven putative mutants capable of transducing retinal pericytes.

Results: Following intravitreal administration of mutant vectors packaging ubiquitously expressing green fluorescent protein reporters and postmortem flow cytometry of enzymatically digested retinae, two mutants in particular, Peri-E and Peri-G, demonstrated significantly greater transduction of retinal pericytes than unmodified rAAV2/2 (1.4-fold and 2.8-fold, respectively).

Conclusions: Although difficult to characterize the effect of each point mutation in the context of multiple amino acid variations from the wild-type AAV2 sequence, we identified several point mutations that may play critical roles in limiting HSPG binding, evading neutralization by murine A20 monoclonal antibodies, modulating antigenicity, and evading ubiquitination to ultimately improve transduction efficiency of retinal pericytes.

Translational Relevance: Identification of novel retinal pericyte targeting rAAV vectors enables the development of new, long-lasting gene therapies for retinal diseases such as diabetic retinopathy and wet age-related macular degeneration.

Introduction

Retinal pericytes are a heterogeneous population of cells derived from mesodermal and neuroectodermal germ layers that play critical structural and physiologic roles in maintaining neurovascular health within the retina.[1] Indeed, retinal pericytes are an essential structural component of the blood–retinal barrier (BRB) that work to regulate endothelial cell proliferation and angiogenesis, and they modulate microvascular blood flow by constricting or relaxing from their perivascular positions on the abluminal surface of capillary blood vessels.[2]

Loss or dysfunction of retinal pericytes is often associated with severe ocular disease, such as in diabetic retinopathy, for which studies have shown an association between reduced retinal pericyte coverage

and increased vascular permeability, pathologic neovascularization, macular edema, and non-perfusion.[3–6] Similarly, loss of pericytes contributes to breakdown of the inner BRB in diseases such as uveitis and age-related macular degeneration, and systemic pericyte dysfunction in the brain and spinal cord has been reported in Alzheimer's disease,[7–9] multiple sclerosis,[10] and amyotrophic lateral sclerosis.[11]

As a consequence, targeting retinal pericytes via gene therapy with the aim of preventing dysfunction or cell death offers an attractive therapeutic opportunity to potentially ameliorate the progression of severe sight-threatening diseases. Unfortunately, due primarily to the broad heterogeneity of pericytes within the retina—where several subclasses coexist and exhibit differential mRNA and cell surface marker expression—targeting pericytes has proven extremely challenging with recombinant adeno-associated virus (rAAV) vectors. rAAV vectors are the most widely utilized tool for transferring genetic material to the retina and have been demonstrated to be safe and effective in numerous preclinical and clinical studies, including for the treatment of inherited retinal disease, such as Leber's congenital amaurosis,[12,13] Leber's hereditary optic neuropathy,[14] and choroideremia.[2,15,16]

In order to overcome this challenge, herein we have used a library screening approach to identify novel rAAV capsid mutant vectors capable of transducing retinal pericytes following intraocular delivery. This technique, where genetic modifications are introduced into the surface of the AAV capsid in order to alter receptor binding and antigenicity, has led to the discovery of safer and more efficient rAAV vectors with altered tissue tropism, including within the retina.[17–22] Importantly, in contrast to rational design approaches, where small numbers of targeted mutations are introduced with the intention of altering specific properties of the capsid (e.g., to limit proteolytic degradation or improve tissue penetrance), library screening is an agnostic approach that requires no prior understanding of how individual mutations may collectively affect tropism in order to rapidly identify novel variants capable of targeting refractive cell types, such as retinal pericytes.

As such, our approach was to conduct multiple rounds of screening following intravitreal injection of a complex rAAV serotype 2–based combinatorial capsid library in Cspg4-DsRed reporter mice, which have red fluorescent pericytes that can be isolated via flow cytometry in order to facilitate genome recovery and quantification of transduction efficiency. Following three rounds we identified seven putative pericyte targeting vectors, and, using a combination of in vivo imaging, flow cytometry, and postmortem histology, we were able to demonstrate that two mutants had significantly improved transduction of retinal pericytes compared with unmodified rAAV2/2.

Methods

Animals

Age-matched male and female Tg(Cspg4-DsRed.T1)1Akik/J mice were purchased from The Jackson Laboratory (Bar Harbor, ME). Mice were bred and housed in the Biomedical Resource Center at the Medical College of Wisconsin under a 12-hour light/dark cycle with food and water ad libitum. All animal protocols were reviewed and approved by the Medical College of Wisconsin Institutional Animal Care and Use Committee and conform with guidelines of the National Institutes of Health and ARVO Statement for the Use of Animals in Ophthalmic and Vision Research.

Capsid Library

Design and construction of the capsid library CL7 used in this study will be described elsewhere (Boye et al., in preparation). Briefly, it is an improved version of the previously described AAV2-based rationally designed capsid library CL6,[20] with a complexity of at least 1×10^7 (extrapolation from Illumina sequencing of viral DNA suggests $>2 \times 10^7$) but less than 2×10^8 (number of library plasmid molecules extrapolated from colony counts after large-scale transformation). CL7 is actually a 9:1 ratio mix of two libraries, one with mutations in variable regions I, IV, V, VI, and VII and another one with mutations in variable region VIII only. Library construction is illustrated in Supplementary Figure S1.

Library Screening

Fifteen to 20 Cspg4-DsRed reporter mice per round (three rounds in total) received bilateral intravitreal injections of the combinatorial library ($1 \times 10^{9–10}$ vector genome [vg]). DsRed-positive cells were harvested 6 days later by fluorescence-activated cell sorting of enzymatically dissociated retinas, followed by recovery of vector genomes using column DNA purification. Following each round, capsid DNA sequences from DsRed-positive cells were recovered by polymerase chain reaction (PCR). After the first two rounds, an enriched capsid library was generated for the subsequent round of in vivo screening by inserting the PCR products into a plasmid

vector containing the wild-type (wt)-AAV2 genome minus the corresponding capsid gene fragment, using Gibson assembly. A diversification step was added after the second round by mutagenizing variable region VIII in half of the enriched library prior to insertion. Variant enrichment was analyzed from PacBio sequencing using caplib3 (https://github.com/damienmarsic/caplib3) after completing rounds 2 and 3 by comparing recovered sequences with injected sequences.

Vector Production

Preparing Mutant Rep-Cap Plasmids

The candidate mutant AAV2-based rep-cap sequences selected after library screening were synthesized and individually cloned into a pUC57 plasmid by Genewiz (South Plainfield, NJ). Mutant rep-cap DNA sequences were subsequently digested from the donor pUC57 plasmids with restriction enzymes *Hind*III and *Nsi*I (New England Biolabs, Ipswich, MA), isolated (QIAquick Gel Extraction Kit; Qiagen, Hilden, Germany), and ligated (T4 DNA Ligase; New England Biolabs) in to the backbone of the AAV2 rep-cap plasmid (pACG2) to form mutant AAV2-based rep-cap plasmids: pACG2-Peri-A, pACG2-Peri-B, pACG2-Peri-C, pACG2-Peri-D, pACG2-Peri-E, pACG2-Peri-F, and pACG2-Peri-G (Supplementary Fig. S2).

Vector Production

rAAV vector production was performed as described previously.[23–25] Briefly, HEK293T cells were triple transfected with an rAAV helper plasmid (pHelper), a self-complementary (sc) green fluorescent protein (GFP) reporter plasmid with a ubiquitously expressing chicken beta-actin promoter (CBA-scGFP), and an AAV2-based rep-cap plasmid—for either unmodified AAV2 rep-cap plasmid (pACG2) or a mutant rep-cap plasmid encompassing one of seven candidate sequences (pACG2-Peri-A, pACG2-Peri-B, pACG2-Peri-C, pACG2-Peri-D, pACG2-Peri-E, pACG2-Peri-F, and pACG2-Peri-G). Equimolar ratios of plasmids were transfected into HEK293T cells and grown in high-glucose Gibco Dulbecco's Modified Eagle Medium supplemented with 2% fetal bovine serum and 1% antibiotic–antimycotic (Thermo Fisher Scientific, Waltham, MA). rAAV vector purification was performed 72 hours post-transfection by iodixanol density gradient centrifugation and buffer exchange using 100-kDa columns (Amicon, Darmstadt, Germany). Finally, rAAV was washed and eluted in Hank's balanced salt solution containing 0.014% Tween 20, and the titer was calculated using a PicoGreen assay (Thermo Fisher Scientific).[24]

Intraocular Injection and Confocal Scanning Laser Ophthalmoscope Imaging

Intraocular injections and retinal imaging were performed under anesthesia using isoflurane. Initial anesthesia was carried out using 5% isoflurane in 100% oxygen for induction, with the concentration of isoflurane being reduced to 2% for maintenance. Mydriasis was achieved prior to injection by topical placement of eye drops containing 2.5% phenylephrine (Paragon BioTeck, Portland, OR) and 1% tropicamide (Akorn, Lake Forest, IL). During injections, corneal hydration was maintained through the application of eye drops containing 2.5% hypromellose (Gonak; Alcon Laboratories, Fort Worth, TX). Briefly, for cohorts of age-matched male and female Cspg4-DsRed mice ($n = 5$ mice per vector), a 33-gauge needle attached to a 5-µL Hamilton syringe was used to administer bilateral intravitreal injections containing $\sim 1.0 \times 10^{10}$ viral genomes of either the purified rAAV2/2 control vector or one of seven mutant vectors (rAAV2/2 [Peri-A–G]) expressing GFP from the ubiquitous CBA promoter. Three weeks after injection, all study animals were imaged using a custom multiline confocal scanning laser ophthalmoscope (cSLO; modified SPECTRALIS HRA; Heidelberg Engineering, Heidelberg, Germany). The camera was aligned using near-infrared (820-nm) reflectance imaging before retinal images of vector-derived GFP fluorescence (excitation, 482 nm; bandpass, 502–537 nm) and intrinsic DsRed (excitation, 561 nm; high pass, 582 nm) were captured at the level of the intermediate capillary plexus. All images were processed using ImageJ software (National Institutes of Health, Bethesda, MD).[26]

Flow Cytometry

Following euthanasia, retinae were dissected from the posterior eye cup and dissociated in an enzyme mix containing 2 mg/mL Pronase, 2 mg/mL DNase, and 5 mg/mL collagenase at 37°C on a rocking platform for 45 minutes, as described previously.[27] Dissociated cells were fixed with 2% paraformaldehyde (PFA) (Thermo Fisher Scientific) and filtered through a 40-µm nylon mesh cell strainer (Thermo Fisher Scientific). GFP and DsRed expression was quantified using a flow cytometer (BD LSR II; BD Biosciences, Franklin Lakes, NJ). For each dissociated retina 1 million events were recorded using the BD LSR II, with dissociated cells from Cspg4-DsRed–negative (no fluorescence) and un-

injected Cspg4-DsRed (red fluorescence only) mice serving as gating controls. The ratio of $GFP^+/DsRed^+$ cells to total $DsRed^+$ cells gave the transduction efficiency for each eye (~10 eyes per group), and the multiple unpaired *t*-tests determined the statistical significance. Flow data were analyzed using BD FACSDiva acquisition software (BD Biosciences).

Flatmount Histology

Enucleated eyes were briefly incubated in 4% PFA and replaced with phosphate-buffered saline (PBS) before the cornea, anterior segment, and lens were resected under a stereo dissection microscope (SMZ800; Nikon, Tokyo, Japan). Following removal from the eye cup, retinae were incubated in 2% PFA for 15 minutes at room temperature before being rinsed three times in PBS, permeabilized with 0.1% Triton X-100 (Sigma-Aldrich, St. Louis, MO) for 15 minutes and subsequently blocked in PBS containing 5% v/v normal goat serum (R&D Systems, Minneapolis, MN) and 2.5% v/v 10% bovine serum albumin (Sigma-Aldrich) for 1 hour. Samples were incubated with a primary GFP polyclonal antibody (1:500 dilution, A-6455; Invitrogen, Carlsbad, CA) at 4°C overnight. After the retinae were rinsed with wash buffer (PBS containing 0.001% Triton X-100) four times, samples were incubated with secondary antibodies to rabbit IgG pre-labeled with Alexa Fluor 488 (1:2000 dilution, A-21206; Invitrogen). Retinae were finally rinsed with wash buffer four times, mounted on microscope slides (Fisherbrand Superfrost; Thermo Fisher Scientific) before being imaged using a confocal microscope (Nikon Eclipse 80i) with a 20× objective and 488-nm and 561-nm lasers (Coherent, Santa Clara, CA). The *z*-stacks covering the full thickness of the retina were recorded, and the images were processed using ImageJ.

Results

An rAAV2/2-based capsid mutant library with an initial complexity of $>1 \times 10^7$ total variants was injected intravitreally ($n = 32$ eyes) into C57BL6J × SJL.$Tg^{(Cspg4\text{-}DsRed.T1)1Akik/J+/0}$ reporter mice (herein referred to as Cspg4-DsRed) that express the red fluorescent DsRed protein selectively in neural/glial antigen 2 (NG2)-positive oligodendrocyte progenitor cells, which in the retina represent populations of retinal pericytes and arteriolar smooth muscle cells. After a period of 6 days post-injection to allow for vector binding and internalization (a longer incubation period was not deemed necessary, as the screening requires only that the capsid variants bind retinal pericytes, not that the cells are functionally transduced), Cspg4-DsRed–positive cells (~1000–1500 cells were recoverable cells per eye) were harvested from enzymatically dissociated retinae via flow cytometry, and vector genomes were recovered and amplified in order to generate an enriched second-generation library with reduced complexity. This process was repeated for a further two rounds (Supplementary Fig. S3) on Cspg4-DsRed cohorts of similar size ($n = 30$ and $n = 40$ in rounds 2 and 3, respectively), with a diversification step in variable region VIII added after the second round.

Enrichment scores between the second and third round were computed for each sequence represented by more than one read in the third-round dataset. For each sequence, three scores were calculated, based on whole sequence enrichment, variable region enrichment, and amino acid enrichment. A global score was defined as the sum of the three scores and was used to sort the sequences. Keeping only sequences with a positive value for each score, an arbitrary cut-off of 1.5 for the global score generated a selection of 11 sequences, which showed some conserved motifs in variable regions (VRs) IV, V, VI, and VII (Supplementary Table). Noticing an absence of consensus in VR I and that several sequences were identical outside VR I, it was decided to assign them a common VR I, reducing the size of the selection from 11 to seven sequences. The VR I sequence GAGAS, having the highest enrichment score, was therefore assigned to the sequences that only differed in their VR I. The seven sequences were assigned alphabetical identifiers Peri-A through Peri-G. Analysis of the amino acid sequence changes in each variable region when aligned relative to unmodified rAAV2/2 (Figs. 1A–1C) revealed no particular trend in the distribution of mutations across the variable regions, as all variants exhibited one or more mutations in VR VI, six variants in VR I, five in VR IV, four in VR V, two in VR VII, and only one (Peri-B) in VR VIII. Many of the residues mutated in the candidate pericyte-targeting capsid sequences have been studied previously and are known to play critical roles in the antigenicity, transduction efficiency, tropism, and proteasomal degradation of wt-rAAV2/2 (summarized in the Table).

Having identified seven candidate pericyte-targeting variants through library screening, we next sought to confirm the efficiencies with which each novel variant packages relative to the wt-rAAV2/2 capsid on the basis that modification of the capsid has been shown previously to affect the efficiency of virion assembly.[28,29] Mutant and unmodified rAAV2/2 vectors packaging

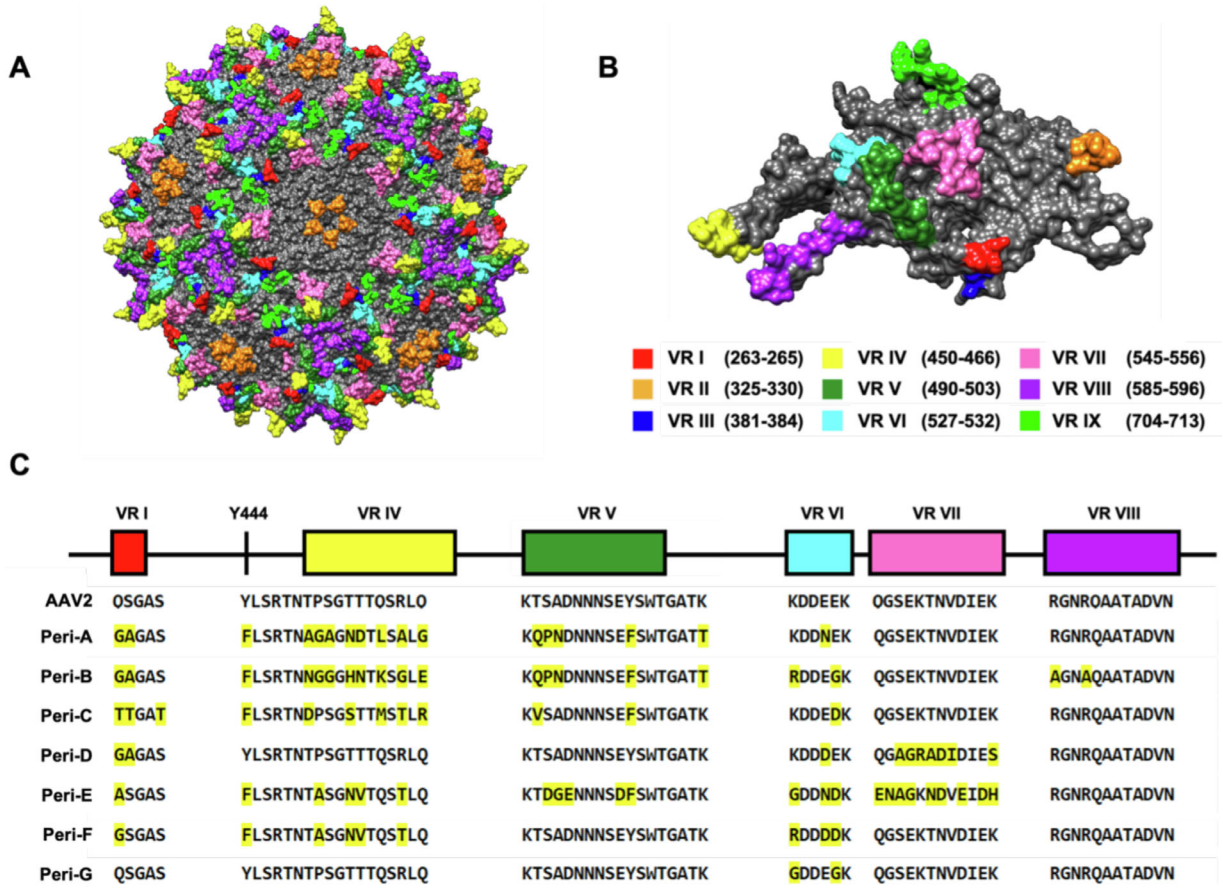

Figure 1. Candidate pericyte-targeting capsid sequences. The assembled AAV2 capsid (A) is composed of 60 subunits (B), each containing nine VRs with amino acid residues localized to the capsid surface. Three rounds of in vivo *s*creening of a rAAV2-based combinatorial library (complexity $>1 \times 10^7$) in Cspg4-DsRed mice led to the isolation of seven capsid variants from DsRed-positive retinal cells. Next-generation sequencing identified specific amino acids (highlighted in *yellow*) mutated from the natural AAV2 cap sequence (C). AAV models were generated using the UCSF Chimera package (supported by NIGMSP41-GM103311).

a CBA–scGFP reporter cassette were produced using a microscale preparation protocol, resulting in the production of six independent batches of purified recombinant virus per vector.[23] The efficiency of virus packaging was assessed first as a function of total vector genome yield per preparation relative to unmodified rAAV2/2 (Fig. 2A), revealing that all pericyte mutant vectors yielded significantly lower numbers of vector genomes, with Peri-C packaging least efficiently (15.6% ± 14.4%; $P < 0.0001$, two-tailed unpaired *t*-test) and Peri-G being most comparable to unmodified rAAV2/2 (69.7% ± 10.5%; $P = 0.0007$, two-tailed unpaired *t*-test). To evaluate, whether poor packaging efficiency was also associated with lower infectivity, HEK293T cells were subsequently transduced with each vector at a multiplicity of infection of 20,000, and GFP expression was evaluated via fluorescence microscopy at 72 hours post-infection, revealing GFP signal in all vectors with the exception of Peri-B, Peri-C, and Peri-F (Figs. 2B, 2C). As a result of the poor packaging efficiencies and low infectivity of these mutants, we elected to conduct further evaluations of variants Peri-A, Peri-D, Peri-E, and Peri-G only.

Preparations of highly purified unmodified rAAV2/2 and mutant vectors Peri-A, Peri-D, Peri-E, and Peri-G were injected intravitreally (1×10^{10} vg/eye in 2 µL) in Cspg4-DsRed mice (10 eyes per vector). In vivo infrared images of the retina captured 21 days post-injection using a cSLO demonstrated no intervention- or vector-induced retinal damage (Fig. 3A). Dual-channel fluorescence imaging revealed intrinsic DsRed expression and widespread vector-derived GFP expression in all eyes examined, with Peri-D and Peri-E demonstrating transduction patterns similar to that of unmodified rAAV2/2, with transgene expression predominantly observed in retinal ganglion cell axons and surrounding the major blood vessels (Fig. 3C). By contrast, Peri-A and Peri-G both demonstrated a more punctate pattern of GFP expression throughout the retina similar to the distribution of

Table. Summary of Critical Residues in the AAV2 Capsid That Influence Antigenicity, Transduction Efficiency, Vector Tropism, and Targeting for Ubiquitination

Variable Region	Residue	Effect/Role	Observed Mutations in Capsid Variants
I	Q263	Target for A20 binding and neutralization[30]	Q263A: Peri-E Q263G: Peri-A, Peri-B, Peri-D, Peri-F Q263T: Peri-C
	S264	Target for A20 binding and neutralization[30] Target for human IVIG[30]	S264A: Peri-A, Peri-B S264T: Peri-C
IV	R459A	Enhanced in vitro transduction of HepG2 and HeLa cells [30]	R459A: Peri-A R459T/G: Peri-B, Peri-C, Peri-E, Peri-F
V	T491	Target for human IVIG[30] Target for phosphorylation and ubiquitination[31]	T491Q: Peri-A, Peri-B T491V: Peri-C
	A493R	Reduced HSPG binding[30]	A493N: Peri-A, Peri-B A493G: Peri-E
	D494	D494A reduced in vitro transduction of HepG2 and HeLa cells[30] D494E enhanced in vitro transduction of HepG2 and HeLa cells[30]	D494E: Peri-E
	Y500	Target for phosphorylation and ubiquitination[32]	Y500F: Peri-A, Peri-B, Peri-C, Peri-E
VI	K527	Target for human IVIG[30] Target for phosphorylation and ubiquitination[33]	K527G: Peri-G
	E530	E530K reduced in vitro transduction of HepG2 and HeLa cells.[30] E530A resulted in viral particles that were defective for transduction.[30]	E530N: Peri-A, Peri-E E530D: Peri-D, Peri-F
	E531	Target for human IVIG[30] Target for human sera[30] E531K reduced in vitro transduction of HepG2 and HeLa cells[30]	E531G: Peri-B, Peri-G E531D: Peri-C, Peri-E, Peri-F
VII	E548	Reduce A20 binding and neutralization[30] Target for human sera[30]	E548G: Peri-D, Peri-E
	T550	Target for human IVIG[30] Target for human sera[30] Target for phosphorylation and ubiquitination[31]	T550A: Peri-D T550N: Peri-E
VIII	R585	HSPG binding[34]	R585A: Peri-B
	R588	HSPG binding[34]	R588A: Peri-B
Miscellaneous	S267T	Enhanced in vitro transduction of HepG2 and HeLa cells[30]	S267T: Peri-C
	Y444	Target for phosphorylation and ubiquitination[32]	Y444F: Peri-A, Peri-B, Peri-C, Peri-E, Peri-F

IVIG, intravenous immunoglobulin.

DsRed retinal pericytes with visibly reduced transduction of retinal ganglion cell axons (Figs. 3B, 3C). Subsequent flow cytometry analysis performed on dissociated retinae from the same rAAV-injected eyes ($n = 10$ per group) revealed a significant increase in the transduction of DsRed-positive cells following intravitreal injection of Peri-E vector (1.4-fold; $P = 0.037$) and Peri-G vector (2.8-fold; $P < 0.0001$) relative

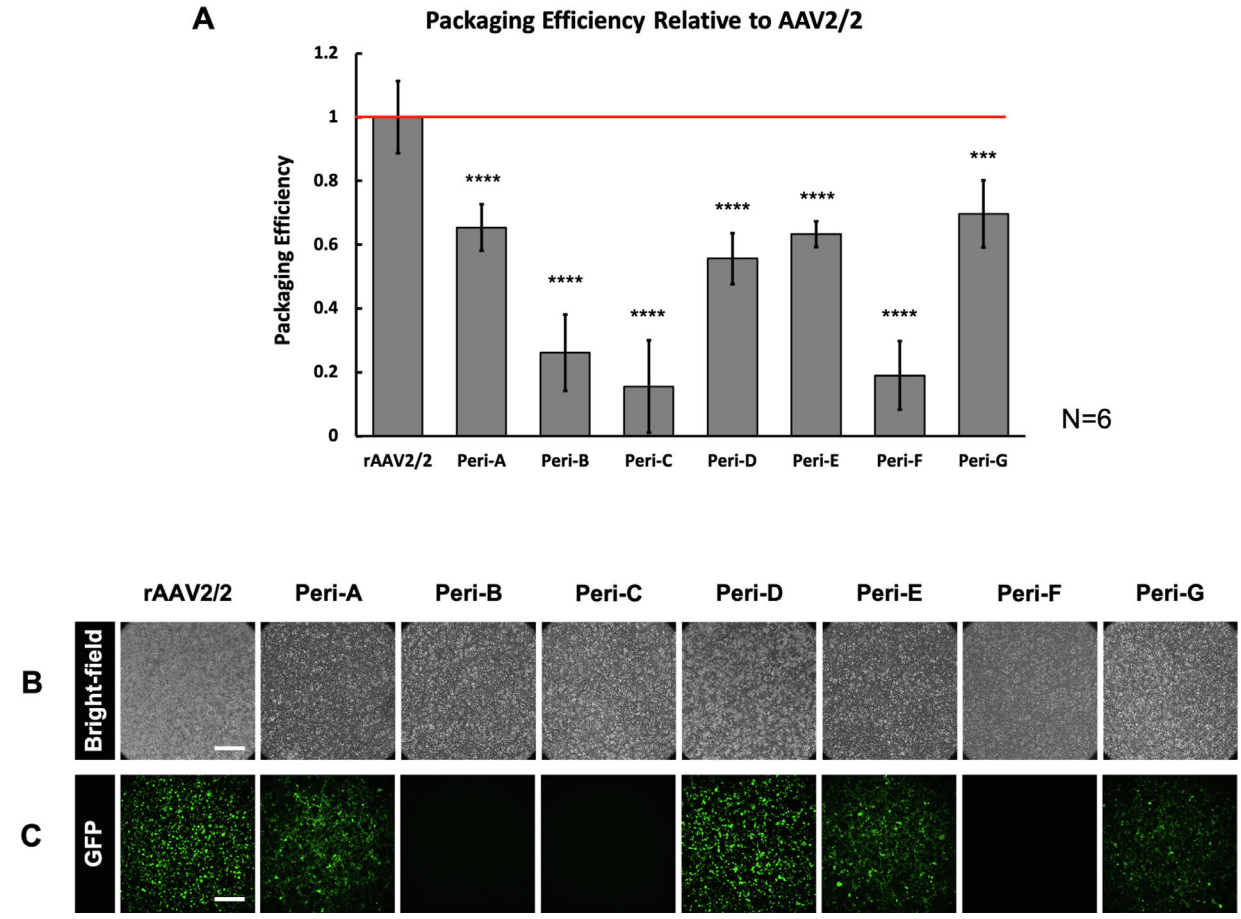

Figure 2. Validating packaging efficiency and infectivity of candidate pericyte-targeting mutant vectors. (A) Following viral production and purification, a PicoGreen fluorescent dye assay was used to quantify the efficiency of DNA encapsidation within each mutant capsid relative to the DNA encapsidation efficiency of unmodified rAAV2/2 ($n = 6$; ****$P < 0.0001$, ***$P < 0.001$, two-tailed unpaired *t*-tests). HEK293T cells were infected with purified vectors (20,000 multiplicity of infection) to assess vector infectivity. Brightfield (B) and respective fluorescence images (exposure time = 500 ms) (C) of HEK293T cells were taken 72 hours post-infection. *Scale bar*: 150 µm.

to eyes injected with unmodified rAAV2/2 (multiple unpaired *t*-tests) (Fig. 3D).

Postmortem histology revealed no detectable GFP expression or obvious autofluorescence in uninjected Cspg4-DsRed eyes (Figs. 4A–4C). Confocal microscopy performed on flatmounted retinae from eyes injected with unmodified rAAV2/2 (Figs. 4D–4F) and Peri-D (Figs. 4K–4M) revealed no or one instance of GFP colocalization with DsRed-positive cells in all three vascular plexi: the superficial vascular plexus located within the retinal ganglion cell layer, the intermediate capillary plexus located within the inner plexiform layer, and the deep capillary plexus, which extends throughout the inner nuclear layer to the outer plexiform layer. By contrast, colocalization of vector-mediated GFP expression with intrinsic DsRed signal was observed throughout in the intermediate capillary plexus and deep capillary plexus of eyes injected with Peri-A (Figs. 4G–4I), Peri-E (Figs. 4M–4O), or Peri-G (Figs. 4P–4S).

Discussion

Loss or dysfunction of retinal pericytes and breakdown of the BRB are implicated in the progression of several ocular diseases, most notably diabetic retinopathy and age-related macular degeneration, so the ability to target retinal pericytes via gene therapy to either correct dysfunction or prevent cell death is an attractive therapeutic avenue.[5] Although rAAV vectors based on naturally occurring serotypes and their capsid mutant derivatives have been demonstrated to safely and effectively transduce numerous retinal cell types, including ganglion cells, Müller glia, several varieties of retinal

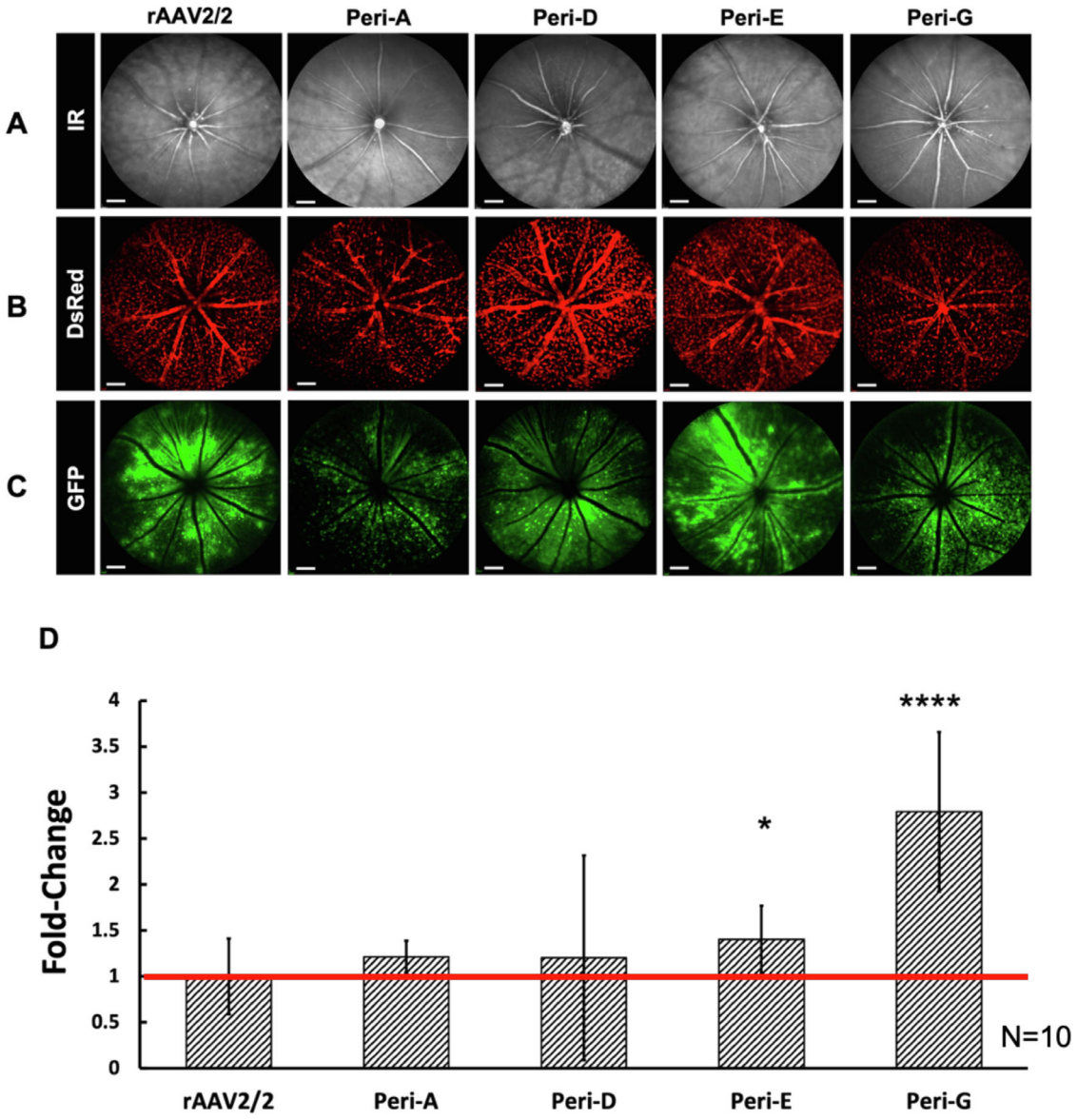

Figure 3. Transduction efficiency of candidate pericyte-targeting vectors. cSLO was used to acquire infrared (A) and fluorescence images of intrinsic DsRed expression (B) and vector-mediated GFP expression (C) in murine retinae, 21 days after intravitreal administration of candidate pericyte-targeting vectors or unmodified rAAV2/2.CBA-scGFP. Retinae were harvested and dissociated into single-cell suspensions, at which point flow cytometry was used to quantify transduction efficiency as the ratio of total GFP^+DsRed^+ cells to total $DsRed^+$ cells. Statistical significance was determined by multiple unpaired *t*-tests. Two-tailed unpaired *t*-tests were used to determine significant differences in transduction efficiency between rAAV2/2 and Peri-E (*$P = 0.037$) and between rAAV2/2 and Peri-G (****$P < 0.0001$). *Scale bar*: 800 µm.

interneurons (e.g., amacrine and bipolar cells), and photoreceptors following intraocular administration, currently we lack a reliable gene transfer vector that can transduce retinal pericytes with high efficiency.[21,35–37]

In order to identify rAAV vectors capable of transducing retinal pericytes, in this study we screened a complex capsid mutant library following multiple rounds of intravitreal injection in a reporter mouse model with DsRed fluorescent protein expressed in retinal pericytes. Importantly, the presence of intrinsic fluorescence in the target cell population allowed for the straightforward isolation and identification of NG2-/Cspg4-positive cells via flow cytometry and microscopy without the necessity of performing immunohistochemistry to detect one or more heterogeneously expressed pericyte markers (e.g., vimentin, αSMA, CD13, desmin), a process that would have likely increased recovery variability and decreased overall yield—a critical consideration when dealing with a rare cell population comprised of ∼7000 to

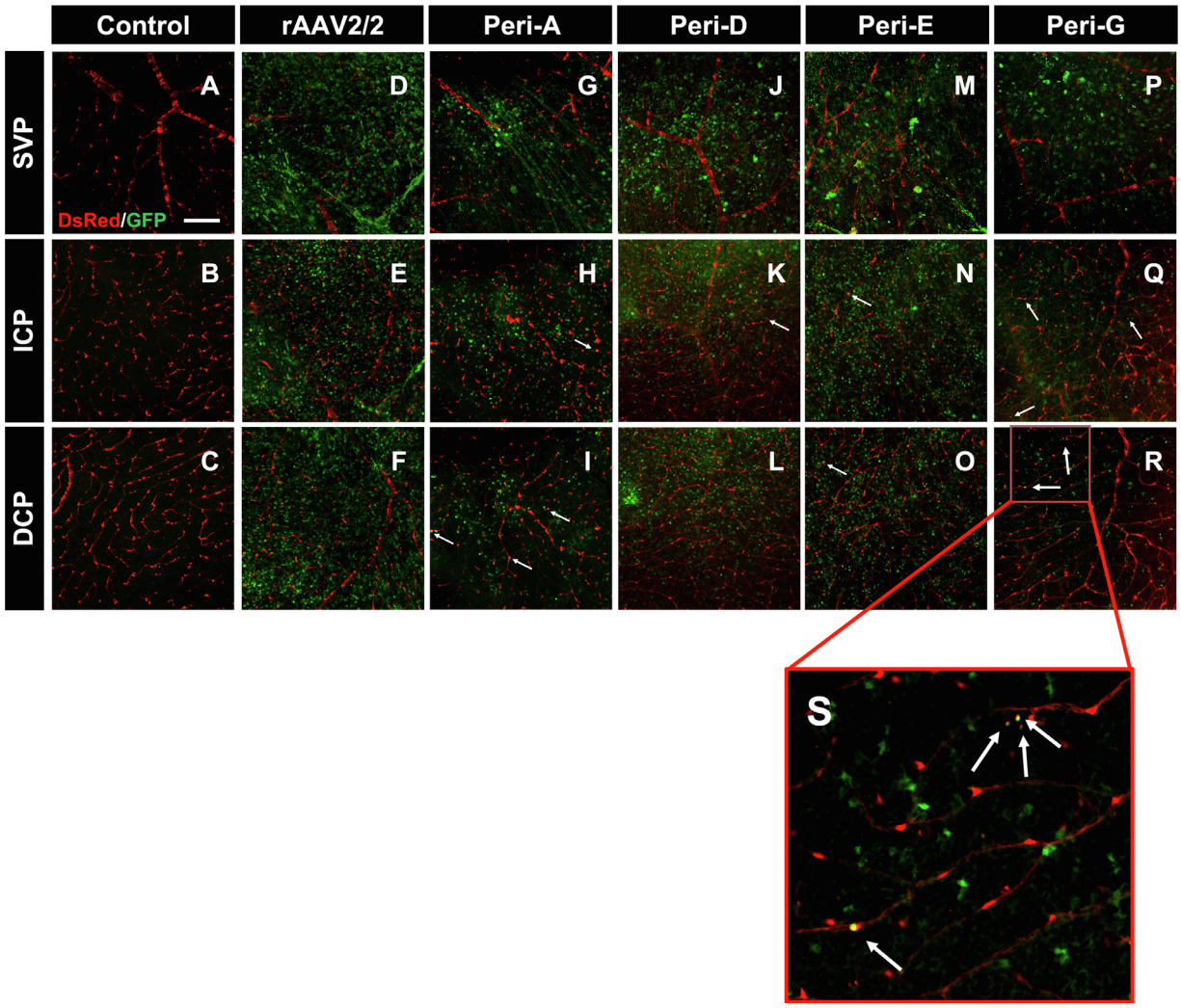

Figure 4. Retinal flatmount histology. Retinae were harvested 21 days after intravitreal administration of unmodified rAAV2/2.CBA-scGFP or candidate pericyte-targeting vectors packaging a ubiquitously expressing GFP reporter cassette. GFP signal was amplified with a primary GFP antibody and Alexa Fluor 488–conjugated secondary antibody. Confocal images at 20× magnification. GFP and DsRed colocalization was evaluated in the superficial vascular plexus (SVP), intermediate capillary plexus (ICP), and deep capillary plexus (DCP). *Scale bar*: 250 µm.

8000 cells in the murine retina (~0.1% of all murine retinal cells).[38,39] Although use of the Cspg4-DsRed model was critical to the outcome of this study, it should be noted that it is possible that not all NG2/Cspg4-DsRed expression in the retina originates from pericytes alone, as NG2 expression from mural progenitors continues even after they differentiate into retinal pericytes and smooth muscle cells of the arterioles.[40] This would be consistent with our observations that DsRed expression on cSLO imaging (Fig. 3B) was most intense surrounding primary and secondary retinal vessels emerging from the optic disk, where the majority of arteriolar smooth muscle cells are expected to be located. A further potential source of DsRed expression in non-pericyte cells is microglia, which, as Wohl et al.[41] demonstrated, also express NG2 following injury-induced cell proliferation or phagocytosis; however, because wild-type animals without damage or degeneration were used throughout this study, we believe this is unlikely to be a substantial source of DsRed positive cells. Moreover, on both cSLO imaging (Fig. 3B) and postmortem flatmount histology (Fig. 4), the majority of DsRed-positive cells were observed to be located at the bifurcations of small retinal vessels—a key characteristic of pericytes—so we are confident that, despite some contamination with NG2-Cspg4–positive arteriolar smooth muscle, the majority of fluorescent cells isolated and examined in this study represent retinal pericytes.

The library injected herein, CL7, was rationally designed as an improved version of the previously described CL6 library, in an attempt to maximize the

number of useful variants.[20] Variable regions II, III, and IX were kept entirely wild type, as it was found that most mutations within them were adversely affecting capsid assembly. Diversification of other variable regions was simplified by removing any mutation that was found to be negatively selected during viral production in the previous version of the library. Finally, mutations in VR VIII were designed as a separate library, with VR VIII being kept wild type in the main library that had mutations simultaneously in VRs I, IV, V, VI, and VII. CL7 was actually a mix of 90% main library and 10% VR VIII library. The rationale for this approach was to allow diversity in a region important for tropism (VR VIII) while keeping high diversity in other regions, knowing that mutations in VR VIII were poorly compatible with the presence of mutations in other regions. Additionally, the idea was to allow those two libraries to compete during earlier rounds of selection and then to add a diversification step by replacing the wild-type regions of the enriched library with the corresponding mutant regions of one of the original libraries. After two rounds of selection, variants in the enriched library had mutations almost exclusively in VRs I, IV, V, VI, and VII. Therefore, the VR VIII of the VR VIII library was used to diversify the enriched library. However, to mitigate the risk of losing valuable variants in case of incompatibility between their mutations and those of the VR VIII library, only half of the enriched library was diversified, the other half being kept wild type in its VR VIII. It turned out that most of the introduced diversity in VR VIII was lost during capsid assembly, with the exception of the R585A and R588A mutations (known to disrupt heparan sulfate proteoglycan [HSPG] binding),[34] and even these were strongly selected against during the third round of selection (Supplementary Fig. S4). This observation confirms previous reports on the importance of HSPG binding for efficient retinal transduction through the intravitreal route of administration.[42] The only candidate with a non–wild-type VR VIII was Peri-B (Fig. 1), which had both low packaging efficiency and low transduction efficiency (Fig. 2).

Interestingly, the most successful candidate variant, Peri-G, was also the one with both the smallest number of mutations and the largest number of wild-type variable regions (Fig. 1). This highlights a recurring dilemma in capsid library design: Larger numbers of alterations to the capsid surface are expected to increase the likelihood of evading preexisting neutralizing antibodies, as well as, at least intuitively, to more significantly alter native tropism. On the other hand, increasing the number of mutations also increases the risk of adversely interfering with capsid assembly or stability, resulting in inferior variants with poor manufacturability. Therefore, it is essential, as is the case with CL7, to allow some level of wild-type sequence for each diversified variable region, resulting in a wide range of numbers of mutations per variant. A consequence of allowing wild-type sequences for VR IV and VR V was the loss, in the variants happening to inherit them, of the Y444F and Y500F mutations that were introduced to increase transduction efficiency by preventing proteasome-mediated degradation.[43] As a result, it is not clear whether the increased efficiency of an improved variant with mutant VR IV or VR V is due to the particular motif present in the VR or just to the Y444F or Y500F mutation. A future version of the CL7 library should include those two mutations in all variants, including those in which the corresponding VR is otherwise wild type.

Due to the complex interaction of the multiple capsid mutations present in each of the variants generated in this study, it is difficult to assign what role, if any, specific mutations may have contributed toward increased transduction efficiency, although the known effects of several mutations are summarized in the Table. A possible exception to this may be Peri-G, which demonstrated a highly significant ($P < 0.0001$) 2.8-fold increase in pericyte transduction despite having only two substitutions (K527G and E531G) in VR VII. To the authors' knowledge, however, these specific mutations have not previously been described in the rAAV capsid, so their role remains unclear. One hypothesis is that, as the Peri-G variant lacks mutations in Y444F and Y500F, which act to protect against tyrosine phosphorylation and subsequent proteasomal degradation, the K527G substitution may compensate by similarly reducing lysine phosphorylation, leading to an improvement in transduction efficiency.[33] Indeed, through a K527E substitution in the wt-AAV2 capsid sequence, Li et al.[33] demonstrated that the transduction efficiency of murine hepatocytes increased by ~8-fold relative to wt-rAAV2/2. Due to the absence of the Y444F and Y500F mutations in some of the variants, including Peri-G, it is possible that reintroducing these substitutions may further enhance the capabilities of each mutant for transducing retinal cells, including pericytes.[44]

Conclusions

Targeting retinal pericytes for gene transfer may benefit the study and treatment of ocular diseases resulting from pericyte loss or vascular dysfunction. Herein we screened a combinatorial library of

$>1 \times 10^7$ AAV2-based capsid mutants in Tg(Cspg4-DsRed.T1)1Akik/J mice, which express DsRed in retinal pericytes, and identified seven candidate pericyte-targeting capsid mutants. Following intravitreal administration of unmodified rAAV2/2 and mutant vectors packaged with a ubiquitously expressing GFP reporter cassette, we identified two capsid mutant vectors that demonstrated significantly enhanced retinal pericyte transduction in vivo (i.e., Peri-E and Peri-G). It is challenging to characterize the effect of each point mutation on receptor binding, antigenicity, and transduction in the context of multiple amino acid variations from the wt-AAV2 sequence. However, we have identified several point mutations that may play critical roles in limiting HSPG binding, evading neutralization by murine A20 monoclonal antibodies, and evading ubiquitination and which could improve transduction efficiency.

Acknowledgments

Supported in part by grants from the National Eye Institute (R01EY027767 and T32EY014537) and the National Institute of General Medical Sciences (T32GM080202) and by a McPherson Eye Research Institute Vision Research Trainee Grant (to DDP). This investigation was conducted in part in a facility constructed with support from a Research Facilities Improvement Program (Grant Number C06RR016511) from the National Center for Research Resources of the National Institutes of Health. The content is solely the responsibility of the authors and does not necessarily represent the official views of the National Institutes of Health.

Disclosure: **D.D. Patel**, None; **D. Marsic**, None; **R. Periasamy**, None; **S. Zolotukhin**, None; **D.M. Lipinski**, None

* DDP and DM contributed equally to this work.

References

1. Trost A, Schroedl F, Lange S, et al. Neural crest origin of retinal and choroidal pericytes. *Invest Ophthalmol Vis Sci.* 2013;54:7910–7921.
2. Trost A, Lange S, Schroedl F, et al. Brain and retinal pericytes: origin, function and role. *Front Cell Neurosci.* 2016;10:20.
3. Mizutani M, Kern TS, Lorenzi M. Accelerated death of retinal microvascular cells in human and experimental diabetic retinopathy. *J Clin Invest.* 1996;97:2883–2890.
4. Hammes HP, Feng Y, Pfister F, Brownlee M. Diabetic retinopathy: targeting vasoregression. *Diabetes.* 2011;60:9–16.
5. Klaassen I, Van Noorden CJF, Schlingemann RO. Molecular basis of the inner blood-retinal barrier and its breakdown in diabetic macular edema and other pathological conditions. *Prog Retin Eye Res.* 2013;34:19–48.
6. Beltramo E, Porta M. Pericyte loss in diabetic retinopathy: mechanisms and consequences. *Curr Med Chem.* 2013;20:3218–3225.
7. Halliday MR, Rege SV, Ma Q, et al. Accelerated pericyte degeneration and blood-brain barrier breakdown in apolipoprotein E4 carriers with Alzheimer's disease. *J Cereb Blood Flow Metab.* 2016;36:216–227.
8. Sagare AP, Bell RD, Zhao Z, et al. Pericyte loss influences Alzheimer-like neurodegeneration in mice. *Nat Commun.* 2013;4:2932.
9. Farkas E, De Jong GI, De Vos RA, Jansen Steur EN, Luiten PG. Pathological features of cerebral cortical capillaries are doubled in Alzheimer's disease and Parkinson's disease. *Acta Neuropathol.* 2000;100:395–402.
10. Kunz J, Krause D, Gehrmann J, Dermietzel R. Changes in the expression pattern of blood-brain barrier-associated pericytic aminopeptidase N (pAP N) in the course of acute experimental autoimmune encephalomyelitis. *J Neuroimmunol.* 1995;59:41–55.
11. Winkler EA, Sengillo JD, Sullivan JS, Henkel JS, Appel SH, Zlokovic BV. Blood-spinal cord barrier breakdown and pericyte reductions in amyotrophic lateral sclerosis. *Acta Neuropathol.* 2013;125:111–120.
12. Bainbridge JWB, Smith AJ, Barker SS, et al. Effect of gene therapy on visual function in Leber's congenital amaurosis. *N Engl J Med.* 2008;358:2231–2239.
13. Cideciyan AV, Hauswirth WW, Aleman TS, et al. Human RPE65 gene therapy for Leber congenital amaurosis: persistence of early visual improvements and safety at 1 year. *Hum Gene Ther.* 2009;20:999–1004.
14. Feuer WJ, Schiffman JC, Davis JL, et al. Gene therapy for Leber hereditary optic neuropathy initial results. *Ophthalmology.* 2016;123:558–570.
15. He L, Vanlandewijck M, Raschperger E, et al. Analysis of the brain mural cell transcriptome. *Sci Rep.* 2016;6:35108.
16. MacLaren RE, Groppe M, Barnard AR, et al. Retinal gene therapy in patients with choroi-

deremia: initial findings from a phase 1/2 clinical trial. *Lancet.* 2014;383:1129–1137.
17. Lipinski DM, Reid CA, Boye SL, et al. Systemic vascular transduction by capsid mutant adeno-associated virus after intravenous injection. *Hum Gene Ther.* 2105;26:767–776.
18. Boye SL, Bennett A, Scalabrino ML, et al. Impact of heparan sulfate binding on transduction of retina by recombinant adeno-associated virus vectors. *J Virol.* 2016;90:4215–4231.
19. Naso MF, Tomkowicz B, Perry WL, Strohl WR. Adeno-associated virus (AAV) as a vector for gene therapy. *BioDrugs.* 2017;31:317–334.
20. Marsic D, Govindasamy L, Currlin S, et al. Vector design tour de force: integrating combinatorial and rational approaches to derive novel adeno-associated virus variants. *Mol Ther.* 2014;22:1900–1909.
21. Maheshri N, Koerber JT, Kaspar BK, Schaffer DV. Directed evolution of adeno-associated virus yields enhanced gene delivery vectors. *Nat Biotechnol.* 2006;24:198–204.
22. Biswas M, Marsic D, Li N, et al. Engineering and *in vitro* selection of a novel AAV3B variant with high hepatocyte tropism and reduced seroreactivity. *Mol Ther Methods Clin Dev.* 2020;19:347–361.
23. Reid CA, Lipinski DM. Small and micro-scale recombinant adeno-associated virus production and purification for ocular gene therapy applications. *Methods Mol Biol.* 2018;1715:19–31.
24. Piedra J, Ontiveros M, Miravet S, Penalva C, Monfar M, Chillon M. Development of a rapid, robust, and universal PicoGreen-based method to titer adeno-associated vectors. *Hum Gene Ther Methods.* 2015;26:35–42.
25. Zolotukhin S, Byrne BJ, Mason E, et al. Recombinant adeno-associated virus purification using novel methods improves infectious titer and yield. *Gene Ther.* 1999;6:973–985.
26. Schneider CA, Rasband WS, Eliceiri KW. NIH Image to ImageJ: 25 years of image analysis. *Nat Methods.* 2012;9:671–675.
27. Cai J, Jiang WG, Grant MB, Boulton M. Pigment epithelium-derived factor inhibits angiogenesis via regulated intracellular proteolysis of vascular endothelial growth factor receptor 1. *J Biol Chem.* 2006;281:3604–3613.
28. Grieger JC, Samulski RJ. Packaging capacity of adeno-associated virus serotypes: impact of larger genomes on infectivity and postentry steps. *J Virol.* 2005;79:9933.
29. Mao Y, Wang X, Yan R, et al. Single point mutation in adeno-associated viral vectors-DJ capsid leads to improvement for gene delivery in vivo. *BMC Biotechnol.* 2016;16:1–8.
30. Lochrie MA, Tatsuno GP, Christie B, et al. Mutations on the external surfaces of adeno-associated virus type 2 capsids that affect transduction and neutralization. *J Virol.* 2006;80:821–834.
31. Aslanidi GV, Rivers AE, Ortiz L, et al. Optimization of the capsid of recombinant adeno-associated virus 2 (AAV2) vectors: the final threshold? *PLoS One.* 2013;8:e59142.
32. Ryals R, Boye S, Dinculescu A, Hauswirth W, Boye S. Quantifying transduction efficiencies of unmodified and tyrosine capsid mutant AAV vectors in vitro using two ocular cell lines. *Mol Vis.* 2011;17:1090–1102.
33. Li B, Ma W, Ling C, Vliet KV, et al. Site-directed mutagenesis of surface-exposed lysine residues leads to improved transduction by AAV2, but not AAV8, vectors in murine hepatocytes in vivo. *Hum Gene Ther Methods.* 2015;26:211–220.
34. Kern A, Schmidt K, Leder C, et al. Identification of a heparin-binding motif on adeno-associated virus type 2 capsids. *J Virol.* 2003;77:11072–11081.
35. Han IC, Cheng JL, Burnight ER, et al. Retinal tropism and transduction of adeno-associated virus varies by serotype and route of delivery (intravitreal, subretinal, or suprachoroidal) in rats. *Hum Gene Ther.* 2020;31:1288–1299.
36. Hellström M, Ruitenberg MJ, Pollett MA, et al. Cellular tropism and transduction properties of seven adeno-associated viral vector serotypes in adult retina after intravitreal injection. *Gene Ther.* 2009;16:521–532.
37. Li W, Asokan A, Wu Z, et al. Engineering and selection of shuffled AAV genomes: a new strategy for producing targeted biological nanoparticles. *Mol Ther.* 2008;16:1252–1260.
38. Jeon CJ, Strettoi E, Masland RH. The major cell populations of the mouse retina. *J. Neurosci.* 1998;18:8936–8946.
39. Schallek J, Geng Y, Nguyen HV, et al. Morphology and topography of retinal pericytes in the living mouse retina using in vivo adaptive optics imaging and ex vivo characterization. *Invest Ophthalmol Vis Sci.* 2013;54:8237–8250.
40. Hughes S, Chan-Ling T. Characterization of smooth muscle cell and pericyte differentiation in the rat retina in vivo. *Invest Ophthalmol Vis Sci.* 2004;45:2795–2806.
41. Wohl SG, Schmeer CW, Friese T, Witte OW, Isenmann S. In situ dividing and phagocytosing retinal microglia express nestin, vimentin, and NG2 in vivo. *PLoS One*. 2011;6:e22408.

42. Woodard KT, Liang KJ, Bennett WC, Samulski RJ. Heparan sulfate binding promotes accumulation of intravitreally delivered adeno-associated viral vectors at the retina for enhanced transduction but weakly influences tropism. *J Virol.* 2016;90:9878–9888.
43. Zhong L, Li B, Mah CS, et al. Next generation of adeno-associated virus 2 vectors: point mutations in tyrosines lead to high-efficiency transduction at lower doses. *Proc Natl Acad Sci USA.* 2008;105:7827–7832.
44. Ran G, Chen X, Xie Y, et al. Site-directed mutagenesis improves the transduction efficiency of capsid library-derived recombinant AAV vectors. *Mol Ther Methods Clin Dev.* 2020;17:545–555.